Electronic Supplementary Information (ESI)

for

Atomic understanding of Formamidinium Hybrid Halide Perovskite, $FAPbBr_3$

Chengmin Li[a], Emilio J. Juarez-Perez[b,c], Alvaro Mayoral[*b,a,d]

a: School of Physical Science and Technology, ShanghaiTech University, Shanghai 201210, China

b: Instituto de Nanociencia y Materiales de Aragón (INMA), CSIC-Universidad de Zaragoza, Zaragoza, 50009, Spain

c: Aragonese Foundation for Research and Development (ARAID). Government of Aragon, Zaragoza, 50018, Spain

d: Laboratorio de Microscopias Avanzadas (LMA), Universidad de Zaragoza, Mariano Esquillor, S/N, 50018, Zaragoza, Spain

Synthesis of Formamidinium Lead Bromide ($FAPbBr_3$)

$FAPbBr_3$ was prepared by simple mechanical mixing. Reagent grade $PbBr_2$ and FABr powders were mixed and crushed in an agate mortar producing a bright orange powder, redissolved in minimal quantity of DMF solvent and precipitated in situ with CH_2Cl_2 solvent. The solid crystalline material on the mortar was carefully collected and filtered off and washed with CH_2Cl_2 solvent and finally dried under vacuum conditions. All reagents were purchased and used as received from Sigma-Aldrich.

Electron microscopy

High-resolution spherical aberration corrected (Cs-corrected) scanning transmission electron microscopy (STEM) was carried out in a X-Field Emission Gun (X-FEG) Titan microscope, equipped with a monochromator, a CEOS corrector for the electron probe (assuring a spatial resolution of 0.8 Å) and a Gatan Tridiem Energy Filter GIF. Sample preparation was performed by grinding the powder using mortar and pestle. After that, the finely divided powder was placed, under dry conditions, onto holey carbon copper microgrids. Due to the high beam sensitivity of the samples a low collection angles was used to obtain the data in order to increase the signal to noise ratio (20-200 mrad). The convergence semiangle employed for the atomic resolution imaging was 15 mrad in all cases. To calculate the electron dose, the beam current was previously measured by using a Faraday cup. Image simulations were performed using QSTEM software. Image simulations of the cubic phase structure were performed from a supercell of 18.11 × 18.11 × 180 $Å^3$. For the tetragonal phase, a supercell of 16.80 × 16.80 × 145.00 $Å^3$ was used for the data simulation. SEM data was collected in a JEOL JEM-7800Prime scanning electron microscope.

3 Dimension-Electron Diffraction Tomography (3D-EDT) data were collected in a JEOL F200 TEM with a Schottky type-emission gun operated at 200kV. To collect the ED patterns with good signal to noise ratio under low electron dose and short exposure time conditions, an ASI Timepix hybrid pixel

detector with 512 ×512 pixel, 55 × 55 μm^2 pixel size was employed. $FAPbBr_3$ sample was dispersed on an ultrathin carbon film copper grid and loaded onto a high-angle single-tilt sample holder. The maximum tilt range of sample holder is from -65° to 65°. All datasets were collected within this range and covered as much as possible. The ED patterns during crystal tilting were recorded in frames with single exposure time 0.3s and total collection time is within 150s. A modified version of the open source *Instamatic 3*[1] software was used for data collection. The collected 3D-EDT data was loaded into *EDT-PROCESS* software[2] and *PETS2.0*[3] software to reconstruct the 3D reciprocal space and extract the reciprocal lattice intensity. The extracted reciprocal intensity was used to solve and refine the crystal structure by *SIR 2019*[4] and *OLEX 2*[5] software.
EDS elemental mapping was collected using a JEOL F200 TEM with a Schottky type-emission gun operated at 200kV equipped with JEOL EDS detector.

Powder X-Ray Diffraction (PXRD)

Powder XRD was performed in a Rigaku SmartLab automated multipurpose X-ray diffractometer equipped with 9 kW rotating anode X-ray source and $K\alpha_1$ optics. $FAPbBr_3$ powder sample was loaded in 0.5mm glass tube. PXRD data was collected in a scan speed of 0.01°/min and the scan step is 0.01°. The experimental data was used to Pawley refine the structure to obtain the precise unit cell parameters, using Topas[6] software.

Morphology of $FAPbBr_3$

The morphology and the relative composition of the as-synthesized $FAPbBr_3$ and of the tetragonal minor phase were also investigated by SEM. From the SEM data it was observed that the major product, $FAPbBr_3$, showed well-defined facets and also wound edges, where the particles were of micrometer size. Furthermore, another type of particles were also detected presenting a slab-like morphology, white arrow Figure S1(b-d), attributed to the tetragonal phase. The major difference is that this minor phase presented a flat surface and short crystal length in the unique direction, typical of a tetragonal symmetry.

Figure S1 a-d) SEM images of $FAPbBr_3$ at different magnifications. a) Major product of $FAPbBr_3$ shows wound edges. b-d) extra phase with relatively less amount marked with white arrows shows slab-lite morphology and flat surface.

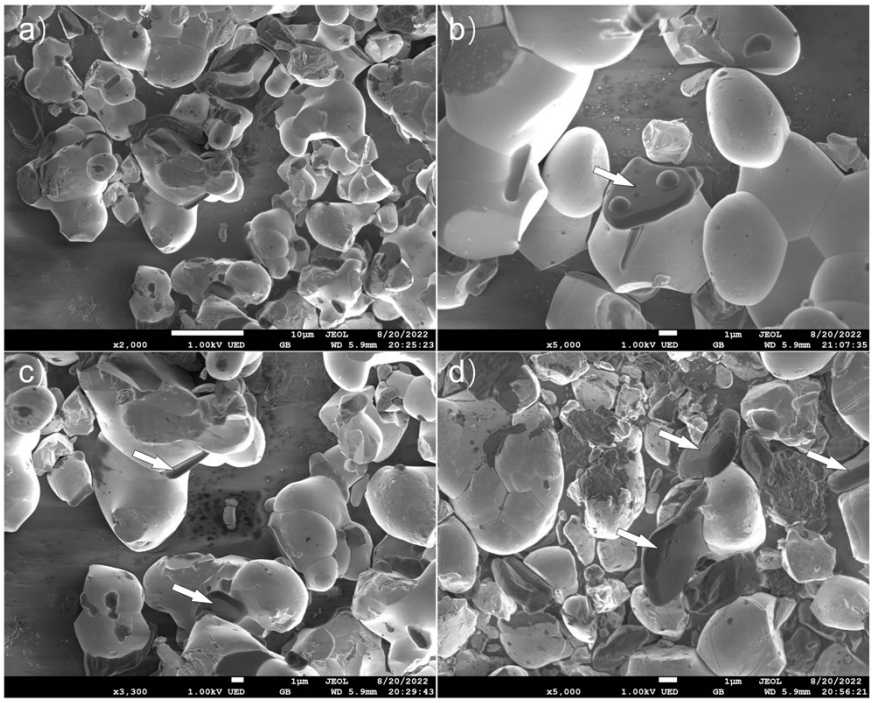
a)
10µm JEOL 8/20/2022
x2,000 1.00kV UED GB WD 5.9mm 20:25:23
b)
1µm JEOL 8/20/2022
x5,000 1.00kV UED GB WD 5.9mm 21:07:35
c)
1µm JEOL 8/20/2022
x3,300 1.00kV UED GB WD 5.9mm 20:29:43
d)
1µm JEOL 8/20/2022
x5,000 1.00kV UED GB WD 5.9mm 20:56:21

3D-EDT datasets

Table S1. Unit cell parameters resulted from the 3D-EDT reconstruction

		a (Å)	b (Å)	c (Å)	α (°)	β (°)	γ (°)
cubic	crystal 1	5.67	5.71	5.69	89.69	90.19	90.32
	crystal 2	5.67	5.72	5.67	89.46	90.05	89.05
	crystal 3	6.15	6.06	5.97	89.49	88.37	91.48
	crystal 4	5.86	5.93	5.99	90.45	91.54	90.00
	crystal 5	5.89	5.91	6.19	90.00	90.00	90.00
	crystal 6	6.09	6.00	5.89	88.95	90.44	91.39
	crystal 7	6.11	5.85	5.91	90.00	90.00	90.00
tetragonal	crystal 8	8.08	8.04	13.80	89.80	89.53	90.01
	crystal 9	8.16	8.11	14.00	90.55	90.48	89.57
	crystal 10	8.48	8.38	14.42	90.35	90.17	90.13
	crystal 11	8.81	8.76	15.15	89.93	91.38	89.91
	crystal 12	8.88	8.92	15.02	90.00	90.00	89.82

Figure S2 3D-EDT datasets identified as cubic structure. Datasets are presented in projection view of the reconstructed 3D reciprocal space. Reciprocal unit cell axis $\boldsymbol{a}^*$, $\boldsymbol{b}^*$ and $\boldsymbol{c}^*$ are marked in red, green, and blue respectively.

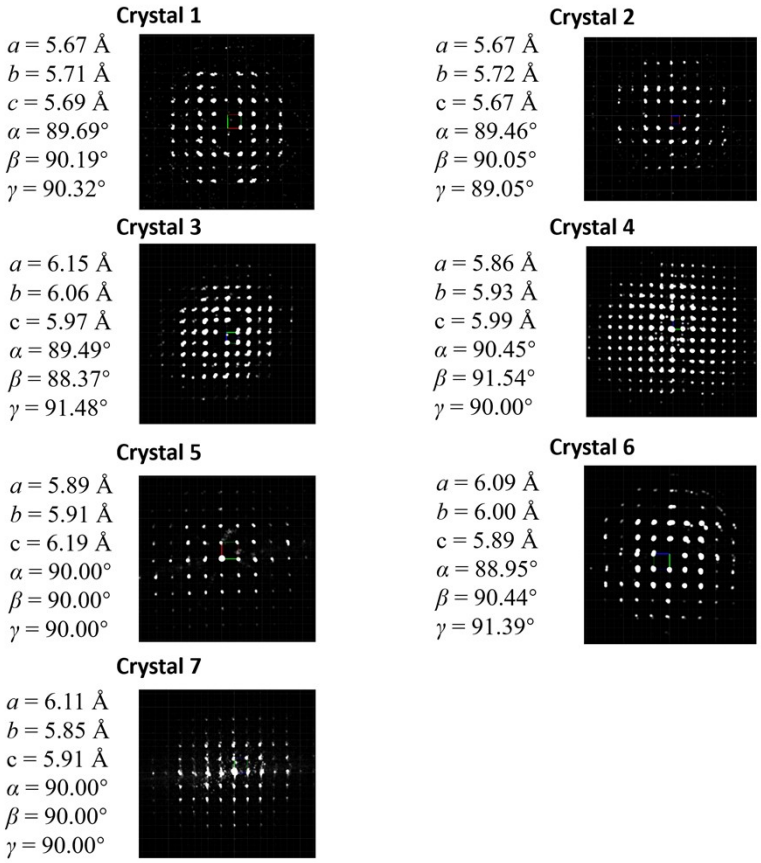

Figure S3 Collected 3D-EDT datasets identified as tetragonal crystal structure. Datasets are presented as the projection view of the reconstructed 3D reciprocal space. Reciprocal unit cell axis $\boldsymbol{a}^*$, $\boldsymbol{b}^*$ and $\boldsymbol{c}^*$ are marked in red, green, and blue.

Crystal 8

a = 8.08 Å
b = 8.04 Å
c = 13.75 Å
α = 89.80°
β = 89.53°
γ = 90.01°

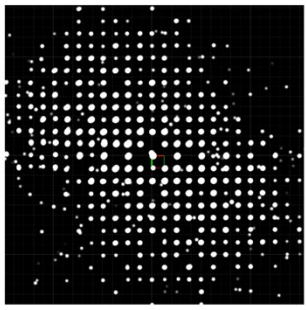

Crystal 9

a = 8.16 Å
b = 8.11 Å
c = 14.00 Å
α = 90.55°
β = 90.48°
γ = 89.57°

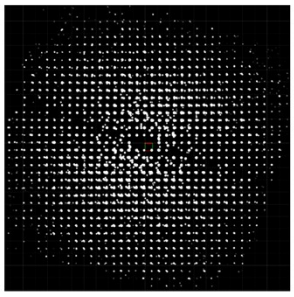

Crystal 10

a = 8.48 Å
b = 8.38 Å
c = 14.42 Å
α = 90.35°
β = 90.17°
γ = 90.13°

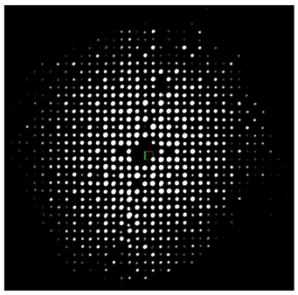

Crystal 11

a = 8.81 Å
b = 8.76 Å
c = 15.15 Å
α = 89.93°
β = 91.38°
γ = 89.91°

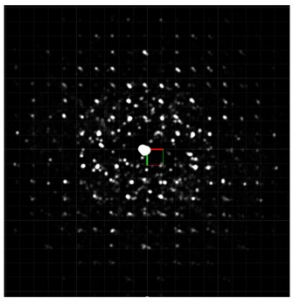

Crystal 12

a = 8.88 Å
b = 8.92 Å
c = 15.02 Å
α = 90.00°
β = 90.00°
γ = 89.82°

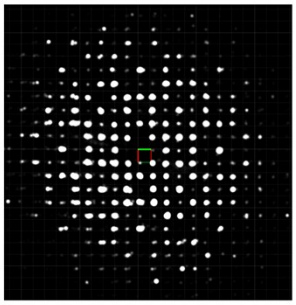

Structure Solution of the Cubic Phase

Table S2. Structure solution after refinement for the cubic phase for $FAPbBr_3$.

formula	CN_2PbBr_3
crystal system	cubic
space group	*Pm*-3*m*
a/Å	5.9968(7)
b/Å	5.9968(7)
c/Å	5.9968(7)
α/°	90
β/°	90
γ/°	90
volume/Å^3	215.65(8)
reflections collected	1738
independent reflections	115 [R_{int} = 0.1967, R_{sigma} = 0.1086]
final R indexes [all data]	R_1 = 0.1617, wR_2 = 0.3271

Collection conditions: Tilting angle -40.90° to 59.27°. Pixel detector records diffraction pattern frames in 0.3s exposure time. The total collection time is 135.5s. 427 frames were processed and extracted to 3470 diffractions.

Figure S4 3D-EDT data used to solve the cubic phase crystal structure. a) Projection view of the reconstructed 3D reciprocal space along 3 axes. b) Slice cut view of reconstructed reciprocal space. This dataset shows a primitive cubic lattice. c) a low magnification view of the crystal where data collected from.

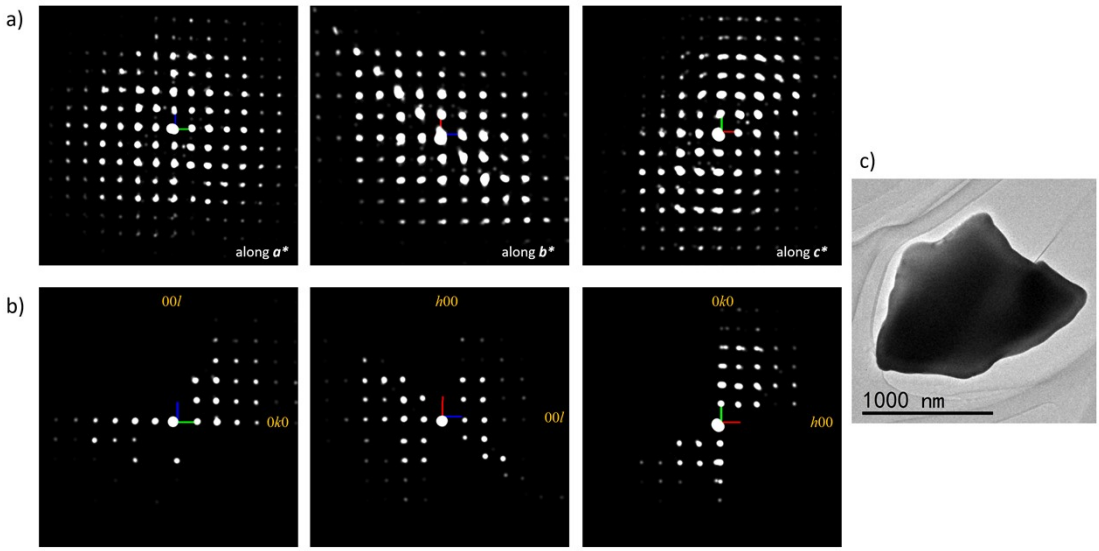

Elemental mapping of $FAPbBr_3$

Figure S5a) shows the electron irradiation sequence of a typical $FAPbBr_3$ crystallite. The top images show a significant shape transformation under electron beam. From 1 to 5, the organic elements, C and N, showed a redistribution along the particle, indicating an organic molecule fading. The Br and Pb signal was detected only from the crystal area during its transformation. Figure S5b) shows a low magnification mapping result before and after electron beam irradiation. The target crystal is marked in red square. From the result it could be found that the Pb and Br are gathering in the remaining crystallite and organic atoms are defusing into surrounding area. Figure S5c corresponds to a $FAPbBr_3$ particle after complete disintegration, in this case the C signal is strongly affected by the grid. For the rest of the elements it can be appreciated the clear formation of individual Pb nanoparticles (on top or below of the final amorphous material formed by C, N, Br and some Pb that did not go into the Pb nanoparticles. The strong morphological transformations indicates that part of the organic compound may be evaporated.

Figure S5 EDS elemental mapping of $FAPbBr_3$ during electron observation. a) Elemental mapping of a 5-stage series. From top to bottom is the crystal outlook image, C, N, Br and Pb mapping. b) Low magnification mapping of this area before and after electron illumination. The target crystal is marked with red square. c) Electron microscopy image and the correspondent chemical maps, showing a homogeneous distribution of the elements, where the Pb nanoparticles can be identified.

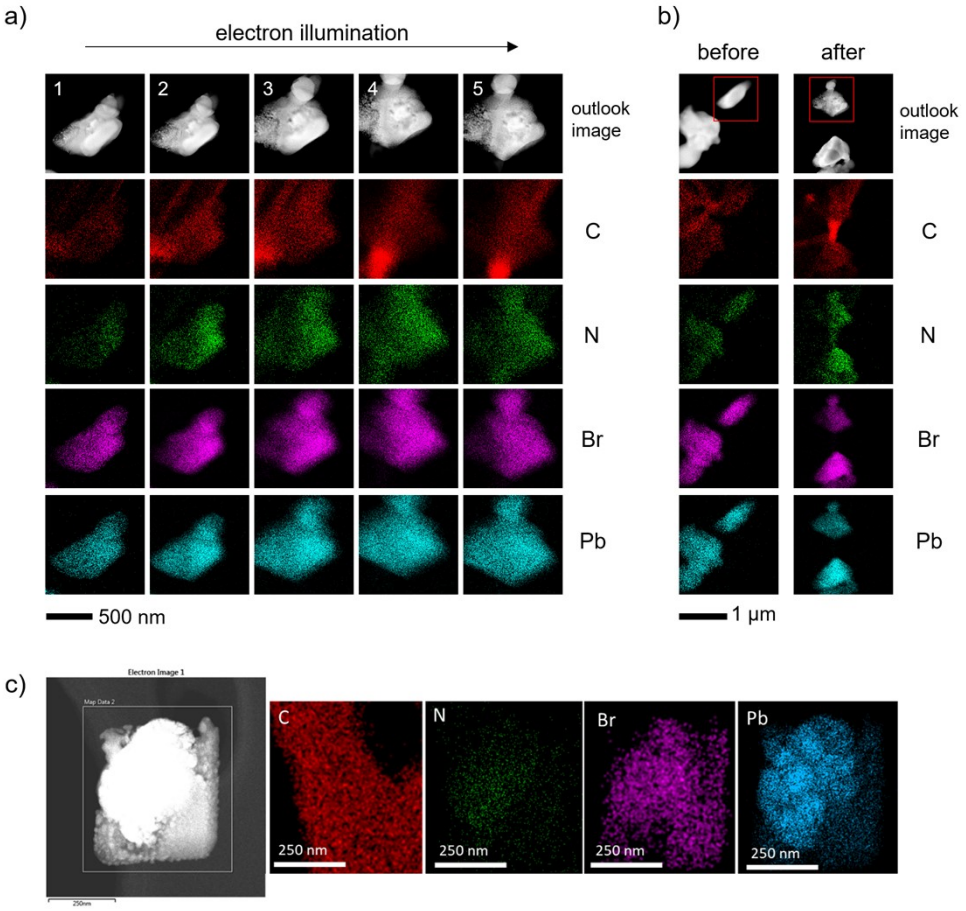

Structure Solution of the Tetragonal Phase

Table S3. Structure solution after refinement for the tetragonal minor phase.

formula	NPb_2Br_5
crystal system	tetragonal
space group	*I*4/*mcm*
a/Å	8.4
b/Å	8.4
c/Å	14.5
α/°	90
β/°	90
γ/°	90
volume/Å^3	1023.1
reflections collected	3904
independent reflections	510 [R_{int} = 0.3020, R_{sigma} = 0.2131]
final R indexes [all data]	R_1 =0.2487, wR_2 = 0.5733

Data collection was from -61.27° to 53.77°, covering 115.05° range. Frames exposure time was 0.3s and total collection time 157.1s. 496 frames were processed and extracted to 4096 diffractions with intensity.

Figure S6 3D-EDT data used to solve the tetragonal phase. a) Slice cut view of the reconstructed reciprocal space through reciprocal space origin (zero order Laue zone). b) Slice cut view of reconstructed reciprocal space of higher order Laue zone. c) a low mag view of the crystal where data collected from. These intensity shows a reflection condition of *hkl* = *h*+*k*+*l; hk*0 = *h*+*k; 0kl* = *k,l; hhl* = *l; 00l* = *l; 0k*0 = *k*. This reflection conditions are in agreement with the Laue class 4/*mmm*.

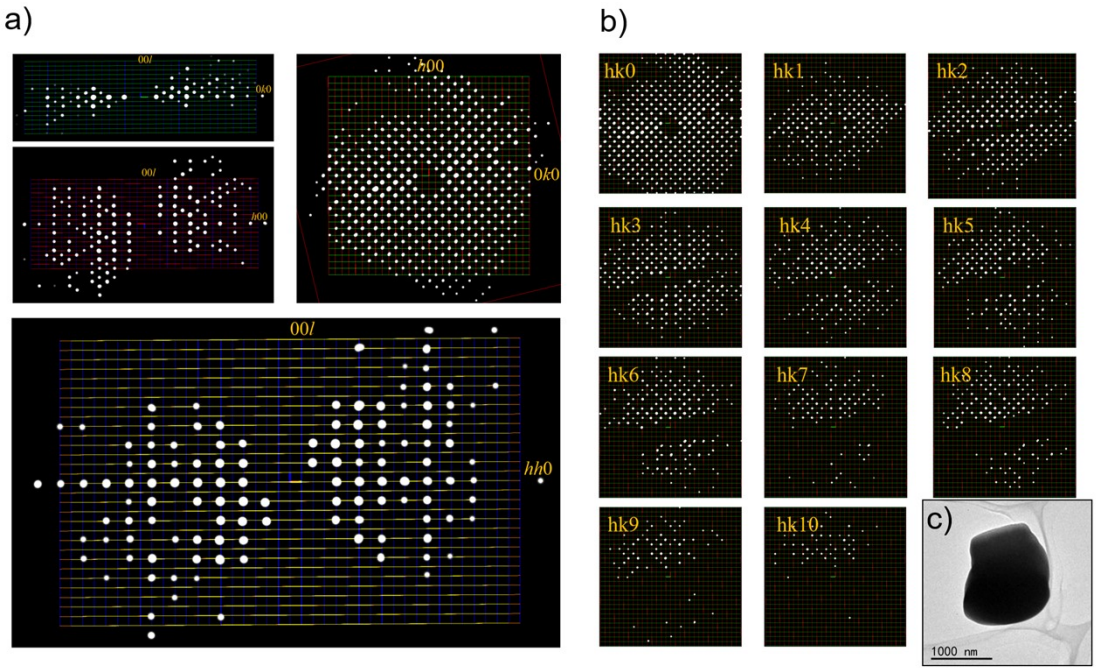

Figure S7 shows the tetragonal phase structure result model solved by 3D-EDT dataset. The solved structure could be regarded as formed by Pb_2Br_5 layers growing in **a** and **b** directions and organic molecules located in **c** direction between two layers, see Figure S7b). Figure S7d) shows the electrostatic potential map reconstructed from 3D-EDT. the white arrows mark a weak potential peak where indicating

a light elemental atom, and it was assigned as N.

Figure S7. A comprehensive view of the tetragonal phase structure solution. a) Along ***c*** axis, b) along ***a*** axis and c) oblique view. d) Electrostatic potential map reconstructed from the 3D-EDT data. Arrows indicate a weak potential signal where light atoms locate, associated to the N. Color code: Pb grey, Br brown and N in blue.

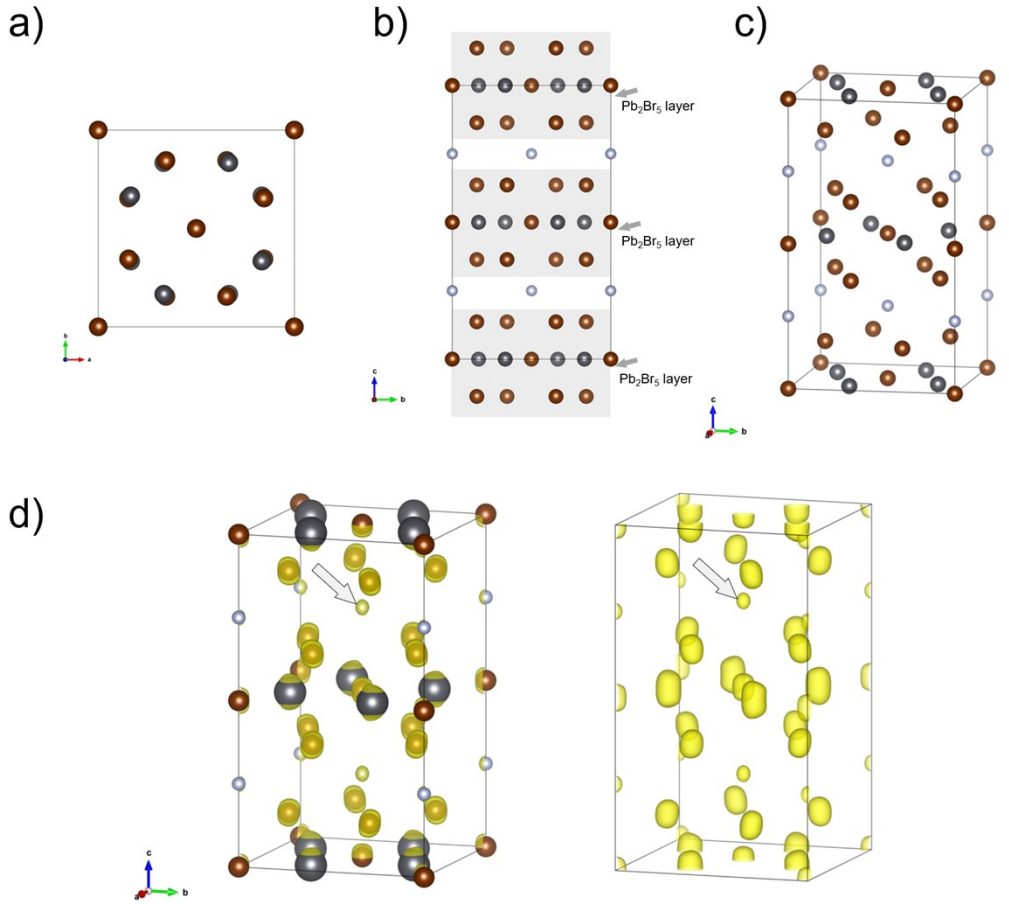

PXRD analysis

PXRD data were acquired to assist on the identification of the two phases. PXRD analysis was employed to refine the structure corroborating the predominant cubic phase with a unit cell parameter of 5.9928 Å and primitive cubic system, red line. The calculated Pawley diffractogram as well as the difference between this one and the experimental data are also presented in Figure S8 (black and blue lines respectively). The Bragg reflections of the calculated cubic phase are marked in green, which could be matched with all major peaks. From the differential diffractogram, additional minor peaks were also observed that did not correspond to the cubic phase. The purple marks are the Bragg reflections calculated from the 3D-EDT structure solution corresponding to the tetragonal phase. Figure S9 shows the 5-50° scan area with index marked. The residual peaks indicating the extra phases including tetragonal phase and other impurities exists with less proportion. The 3D-EDT structure solutions of the cubic and tetragonal phases were also used to make component analysis by Rietveld refinement method, under an approximation of two-phase existence. The proportion result is 95% for cubic phase and 5% for tetragonal phase, indicating the $FAPbBr_3$ cubic phase is the major product.

Figure S8. PXRD spectra of the experimental data, Pawley refinement and Bragg positions of the cubic and tetragonal phases obtained from the EDT data.

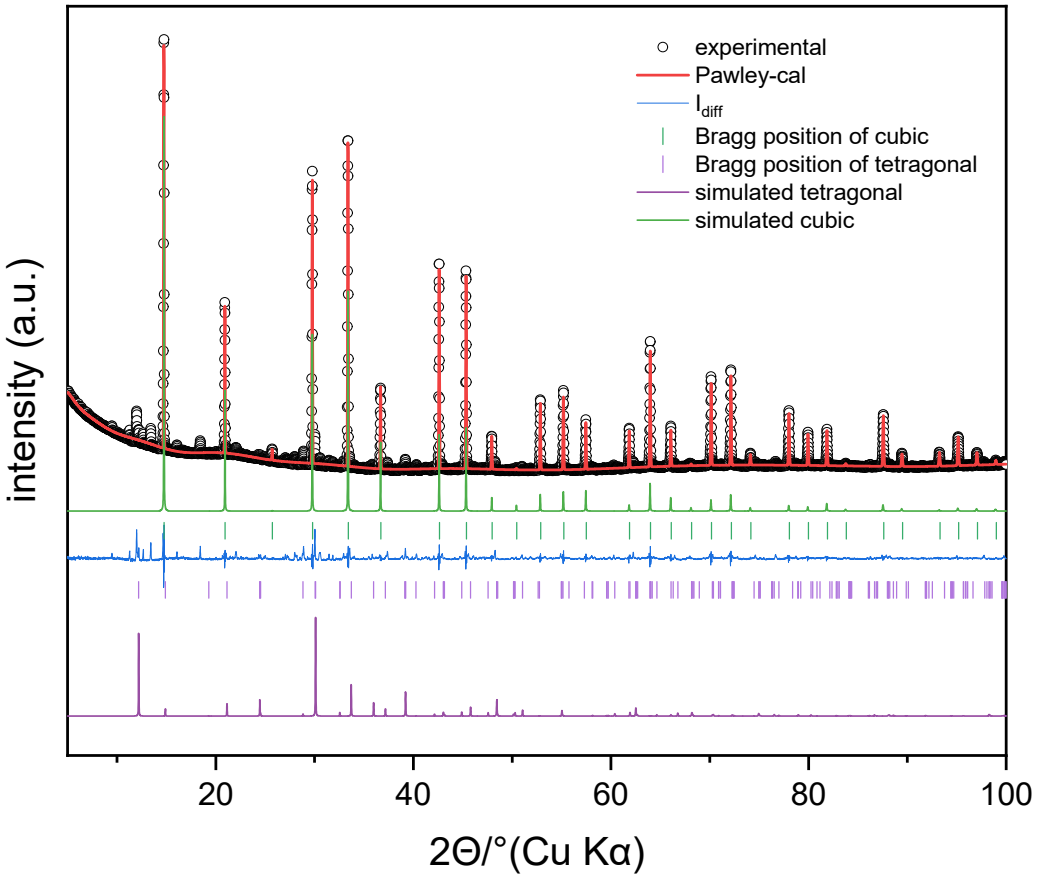

Figure S9. PXRD spectra between 5° to 50° of the experimental data, Pawley refinement and Bragg positions of

the cubic and tetragonal phases obtained from the EDT data. The index of Bragg positions are marked.

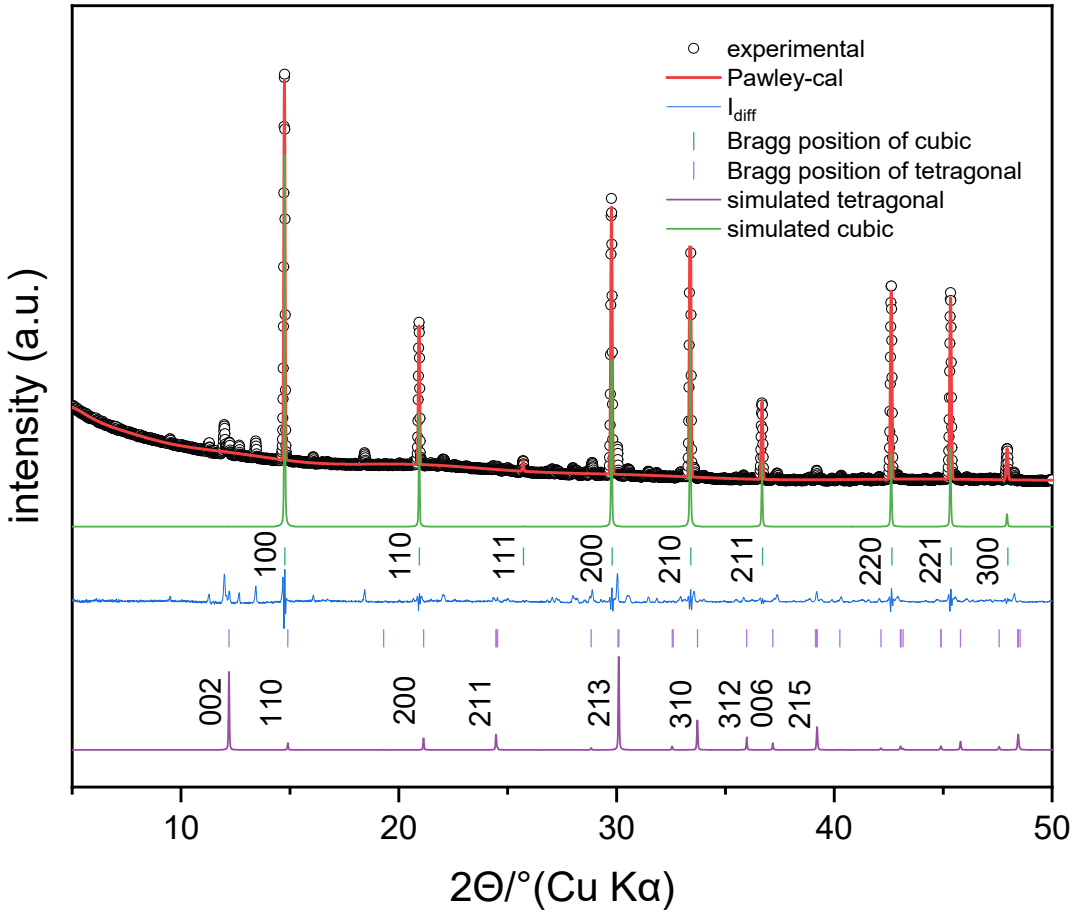

References

1. Smeets, S.; Wang, B.; Cichocka, M.; Ångström, J.; Wan, W., Instamatic. **2018**.

2. Gemmi, M.; Oleynikov, P., Scanning Reciprocal Space for Solving Unknown Structures: Energy Filtered Diffraction Tomography and Rotation Diffraction Tomography Methods. *Zeitschfrift Für Kristallographie* **2013**, *228*, 51-58.

3. Palatinus, L.; Brázda, P.; Jelínek, M.; Hrdá, J.; Steciuk, G.; Klementová, M., Specifics of the Data Processing of Precession Electron Diffraction Tomography Data and Their Implementation in the Program Pets2. 0. *Acta Crystallographica Section B: Structural Science, Crystal Engineering and Materials* **2019**, *75*, 512-522.

4. Burla, M. C.; Caliandro, R.; Carrozzini, B.; Cascarano, G. L.; Cuocci, C.; Giacovazzo, C.; Mallamo, M.; Mazzone, A.; Polidori, G., Crystal Structure Determination and Refinementviasir2014. *J Appl Crystallogr* **2015**, *48*, 306-309.

5. Dolomanov, O. V.; Bourhis, L. J.; Gildea, R. J.; Howard, J. A.; Puschmann, H., Olex2: A Complete Structure Solution, Refinement and Analysis Program. *J Appl Crystallogr* **2009**, *42*, 339-341.

6. Coelho, A., Indexing of Powder Diffraction Patterns by Iterative Use of Singular Value Decomposition. *J Appl Crystallogr* **2003**, *36*, 86-95.